aerospace

MDPI

Article

Development of SMA Spring Linear Actuator for an Autonomous Lock and Release Mechanism: Application for the Gravity-Assisted Pointing System in Moon to Earth Alignment of Directional Devices

Girolamo Costanza [1], Giovanni Ottavio Delle Monache [2,*], Maria Elisa Tata [1] and Stefano Filosi [1]

[1] Industrial Engineering Department, University of Rome Tor Vergata, 00133 Rome, Italy
[2] National Institute of Nuclear Physics Frascati National Laboratory, 00044 Frascati, Italy
* Correspondence: giovanni.dellemonache@lnf.infn.it; Tel.: +39-06-94032544

Abstract: The next generation lunar reflector (NGLR) experiment is one of the experiments selected by NASA in the framework of the commercial lunar payload services (CLPS) initiative. The experiment, inspired by the lunar laser ranging (LLR) experiments of the Apollo era, is basically a single cube corner reflector (CCR) capable of reflecting a beam coming from a laser station on Earth that must be deployed on the Moon and pointed toward the mean Earth direction. In this work, a prototype of an actuator for the lock and release system of the reflector package was conceived, built, and tested in laboratory conditions. Since the entire pointing system must be passive, the actuator is designed to be operated by an SMA spring actuated by the thermal radiation of the Sun and regolith on the Moon. In lab conditions, the prototype, activated by a heat gun, showed the capability of the SMA spring to operate a lock and release pin, whose diameter is 4 mm, subjected to a preload of F = 7 N exerted by the releasing spring.

Keywords: NGLR experiment; gravity-assisted pointing system; shape-memory alloy actuator

check for updates

Citation: Costanza, G.; Delle Monache, G.O.; Tata, M.E.; Filosi, S. Development of SMA Spring Linear Actuator for an Autonomous Lock and Release Mechanism: Application for the Gravity-Assisted Pointing System in Moon to Earth Alignment of Directional Devices. *Aerospace* **2022**, *9*, 735. https://doi.org/10.3390/aerospace9110735

Academic Editor: M. Reza Emami

Received: 11 October 2022
Accepted: 19 November 2022
Published: 21 November 2022

Publisher's Note: MDPI stays neutral with regard to jurisdictional claims in published maps and institutional affiliations.

Copyright: © 2022 by the authors. Licensee MDPI, Basel, Switzerland. This article is an open access article distributed under the terms and conditions of the Creative Commons Attribution (CC BY) license (https://creativecommons.org/licenses/by/4.0/).

1. Introduction

The NGLR experiment is a single CCR whose diameter is 100 mm to be deployed on the Moon's surface. Experiments with CCR for LLR application were deployed during extravehicular activities (EVAs) of Apollo 11, 14, and 15 and on the robotic rover Lunokhod. As reported in [1], Apollo reflectors were manually aligned by astronauts. The Lunokhod has been aligned by remotely maneuvering the rover to a favorable position pointing toward the mean Earth direction.

Differently, the NGLR experiment will be integrated on the lander from the Firefly Aerospace company, named Blue Ghost, a robotic spacecraft selected by NASA within the CLPS initiative, expected to land on the Moon in early 2024.

NGLR is conceived as a low-budget scientific package, and for this reason, in the first stage, the experiment was conceived as a fixed pointing device whose elevation angle is adjusted before the launch, when the landing site on the Moon is defined. In this configuration, the success of the deployment relies on the spacecraft control system during landing and on the capability or chance of the system to land in a favorable morphological configuration.

In this context, a passive pointing system has been proposed by Delle Monache et al. [2], represented in Figure 1, for the next NGLR experiment payload to possibly be deployed on different landing sites. The proposed system does not use an electro-actuated axis (if the azimuthal alignment can be provided by the lander) and can compensate for the clocking and elevation angle by just using the effect of lunar gravity. This represents a set of benefits in terms of reliability (which is crucial for mechanisms on the Moon), development costs, and weight, as evidenced by Dietz et al. in [3]. In its deployed configuration, the

system is not isostatic, so during the launch phase, a lock and release system must be provided for the stowage of the experiment and its structural integrity. In order to passively maintain the system, a solution using an SMA actuator triggered just by solar radiation was investigated and presented in this work. The solution can be applied to any directional device that requires a single pointing capability, such as antennas.

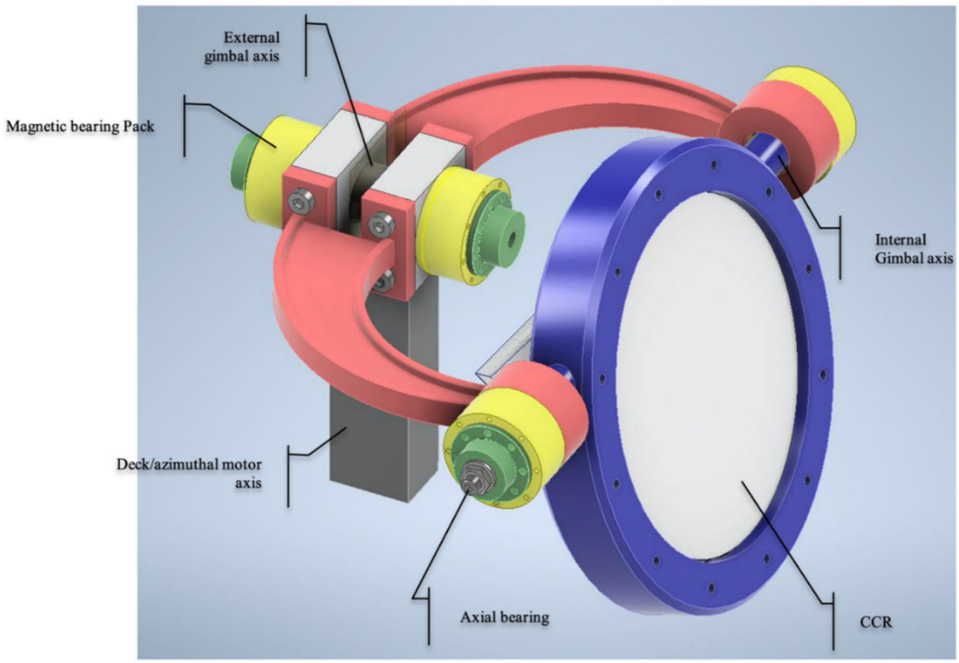

Figure 1. NGLR experiment cardan suspension layout.

2. Materials and Methods

2.1. Shape Memory Alloys Actuators

The shape memory effect is related to the reversible crystalline phase transformation experienced by shape memory alloys at different temperatures [4]. The low-temperature phase is a martensitic structure that can undergo large strain deformation (up to 10% in some alloys) with relatively low stress (approx. 70 MPa) under a high number of activation cycles [5]. The high-temperature stable phase is a cubic-based, austenitic structure whose behavior is that of a conventional metal. When the martensite (monoclinic) is deformed in the cold state and then heated, the original heat-treated shape is recovered. However, if the deformed martensite is constrained while heated, high recovery stress evolves. The use of SMAs in the past has been limited due to a lack of understanding of their force-length-temperature response and their non-linear and hysteretic behavior. In addition to these, also fatigue (mechanical and functional), creep, and material properties drift, which results from transformational cycling, have been the scope of intense research.

In space applications, the strong interest in SMAs derives from the chance offered to design compact and lightweight actuators with limited complexity if compared with standard technologies, as evidenced in a recent review [6]. At present, several SMA actuators are commercially available as space-qualified hardware, in particular for lock and release mechanisms. The developed mechanisms in practical use include separation nuts (micro and mini), a mini rotary actuator, a micro burn wire release, an SMA linear actuator, and an SMA redundant release mechanism. Moreover, in small satellites, a great variety of pull-out systems to accomplish the functions of many missions (separation from the launch vehicle, separation from each other, and instrument deployment) are always more frequently required.

In past years, several solutions with SMA actuators in space applications have been designed, and some of them have used sunlight as an activation heat source [7]. In this

context, the lunar environment with its extreme temperatures represents an important asset if considering a similar solution, keeping in mind that SMA actuators have been developed at liquid nitrogen temperatures as well [8], and, no matter what the landing site is, the lunar environment does guarantee such lower temperature during the lunar night.

2.2. Lock and Release Mechanism for the NGLR Experiment

The proposed solution is based on an actuated pin pulling [9], locked in place during the launch, and actuated by an SMA spring after deployment. A sketch of the system is depicted in Figure 2.

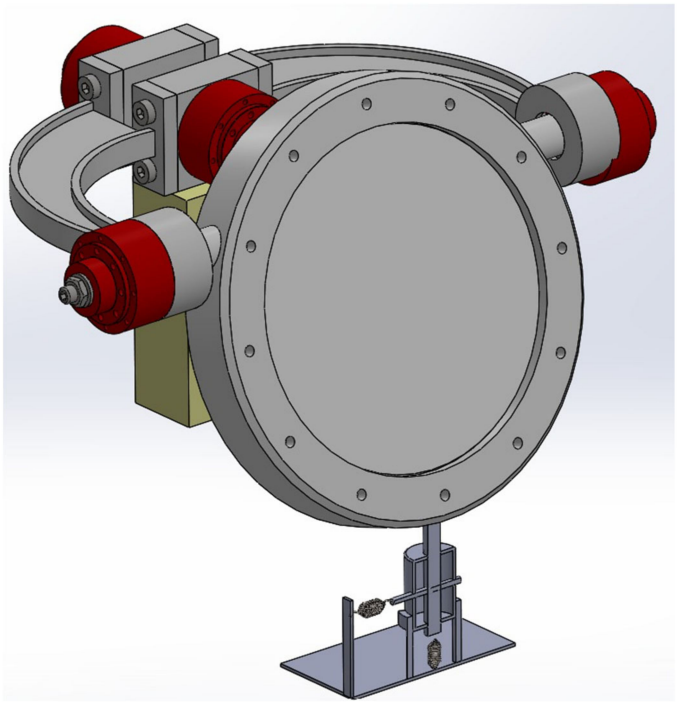

Figure 2. Launch lock and release autonomous mechanisms. The actuated pin collaborates with the structural resistance of the CCR package during the launch.

The actuated pin is inserted in a seat machined on the housing. The detailed design will optimize the properties of the locking pin in terms of contribution to the structure to resist the dynamic load environment of the launch and landing phases once these are defined. When considering the package as a constrained structure, the design will define an isostatic scheme to introduce additional loads due to the temperature gradient in the package during the launch and deployment phases. In the following, the Elegant BradBoard Model (EBB) is described.

The actuator involves the use of two springs, one in harmonic stainless steel and the other in NiTinol. The system consists of the main case that has the purpose of directing the movement of the locking pin. A secondary seat in the case drives a sealing pin, which is inserted into a hole in the locking pin, keeping it in place before the SMA is activated, as shown in Figures 3 and 4. The steel spring is preloaded and anchored to the base plate of the case, while the external anchor of the SMA spring must be defined once the architecture of the lunar lander deck is fixed. No matter what happens, the case can be designed in a way that includes the external SMA spring anchor as well. The principle of operation is very simple and is aimed at eliminating the use of any type of control or electro-handling system. Once the SMA spring is exposed to the activating temperature, the SMA spring pulls the sealing pin away from the locking pin, and the steel spring releases the housing of the reflector, as evidenced in Figure 5.

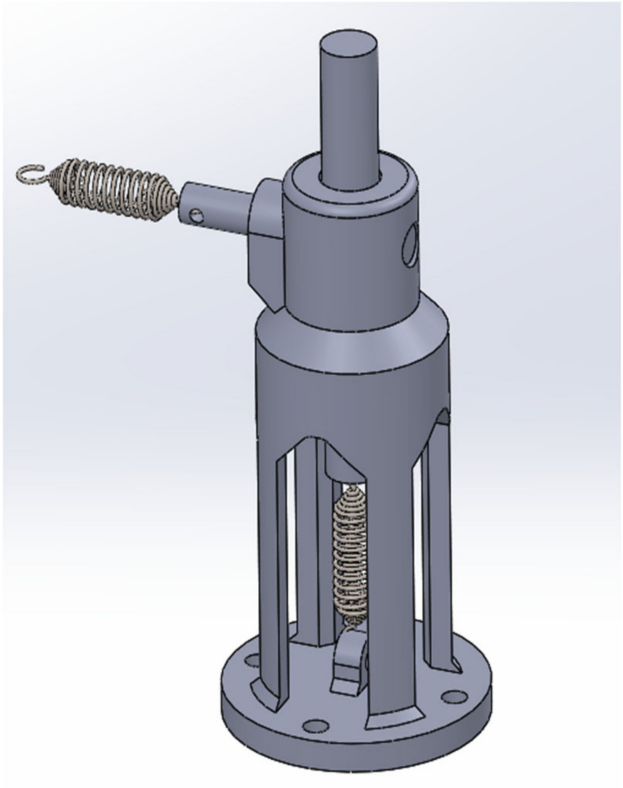

Figure 3. SMA actuator layout.

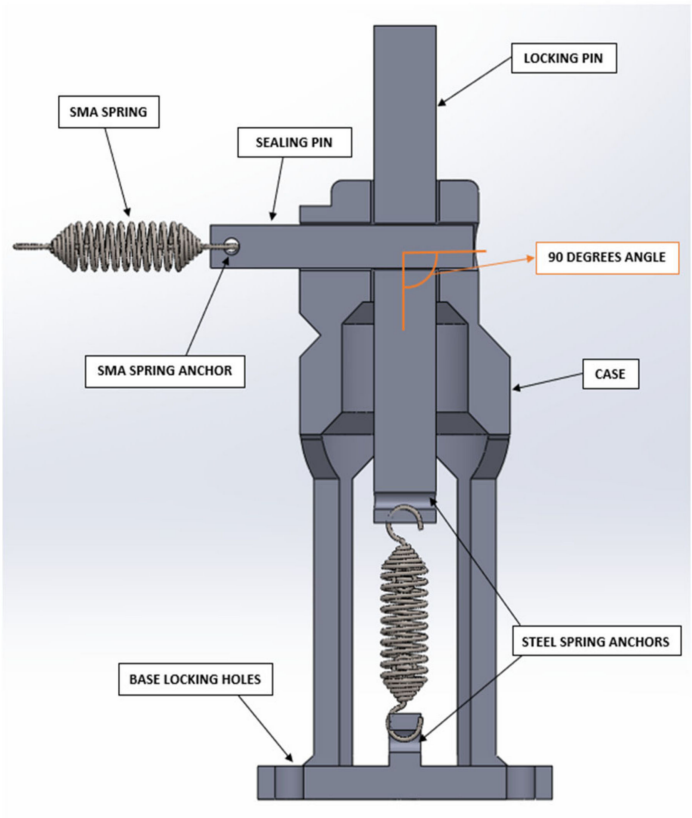

Figure 4. SMA actuator cross-section.

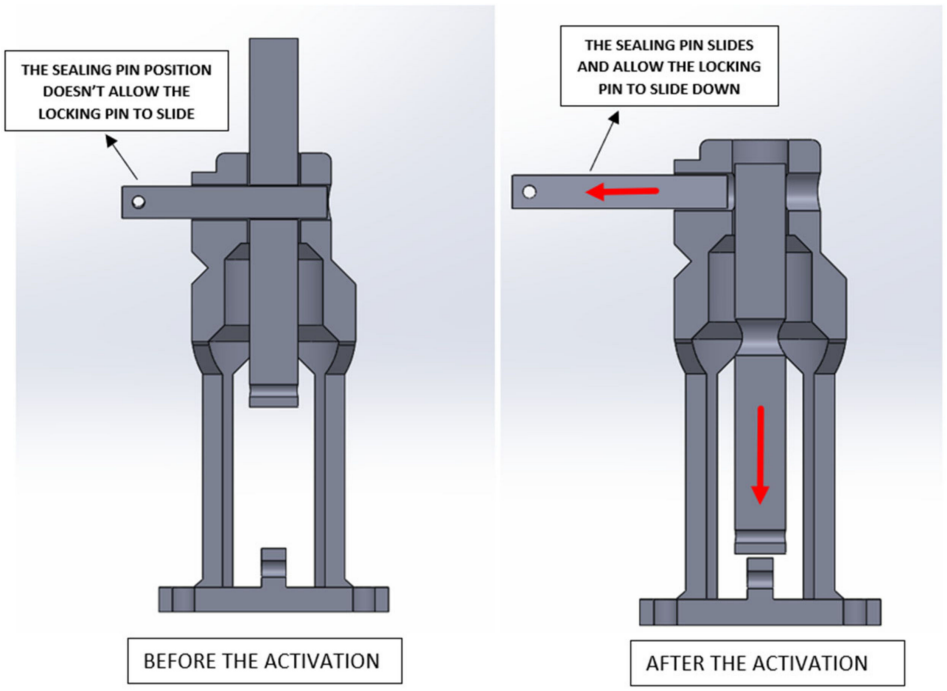

Figure 5. SMA actuator releasing scheme before and after the activation.

The steel traction spring is preloaded, while the SMA spring connected to the sealing pin is activated, recovering its initial shape when a temperature of 65 °C is reached. The steel spring is used to facilitate the release of the locking pin if the lander should land on the lunar soil at a nonzero angle, exerting a force adequately calculated in addition to the force due to the acceleration of lunar gravity.

The housing of the EBB actuator was made using FDM (fused deposition modeling) technology, using a polymer particularly suitable for rapid prototyping by 3D printing, namely PLA (polylactic acid). To verify the correct functioning of the designed apparatus and properly size the two springs used in the system, it is of primary importance to know the friction coefficient that is established between PLA and stainless steel (with which the pins are made). From various articles and experiments of tribological tests found in the literature, a value of $\mu = 0.5$ has been assumed as the friction value for the PLA/steel pair. The real actuation of the lock and release mechanism is performed by the SMA spring. For the EBB NiTinol has been chosen. The main SMA performance parameters are reported in Table 1.

Table 1. SMA spring performance parameters.

Composition (wt %)	Af Temperature (°C)	SMA Wire Diameter (mm)	Spring Mid Diameter (mm)	Number of Turns	$E_{Austenite}$ (GPa)
50 Ni–50 Ti	65	0.8	6	20	72

2.3. SMA Spring Design and Manufacturing

The spring in the prototype must be able to overcome the friction force that is generated at the points of contact between the sealing pin and the supporting PLA structure and between the sealing and locking pins.

The coefficient of friction between steel and PLA does depend on several factors, such as PLA quality and print orientation as shown in Figure 6 [10].

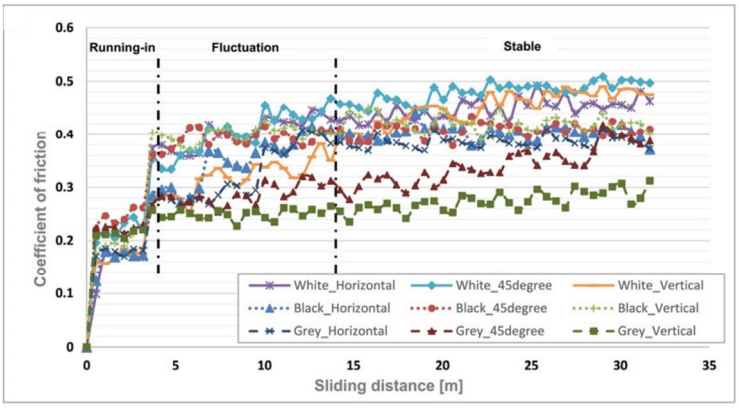

Figure 6. PLA/steel friction behavior curves [10].

In order to estimate the friction force to be overcome by the SMA spring, as mentioned above, a conservative coefficient of friction equal to $\mu = 0.5$ for the PLA/steel pair was assumed.

Having already chosen and characterized the booster spring, it is well known the load the sealing pin is subjected to; thus, we are able to calculate the starting friction force that the SMA spring must overcome to trigger the release of the system, which corresponds to $F_{att} = 2.9\ N$. In addition to the calculation, the starting force has been measured with a calibrated Sauter digital force gauge. Experimental results are in very good agreement with the theoretical ones (+/−2%).

After preliminary testing, a wire with a diameter equal to 0.8 mm coiled in 20 turns was built, requiring a minimum stroke of 25 mm.

In principle, the performances of an SMA spring in the martensitic-austenitic transition cab can be analytically determined.

With reference to Figure 7, the output force at temperature T can be obtained [11,12].

$$F(T) = \frac{G(T)d^4}{8\,D^3\,n}\,\delta_L \tag{1}$$

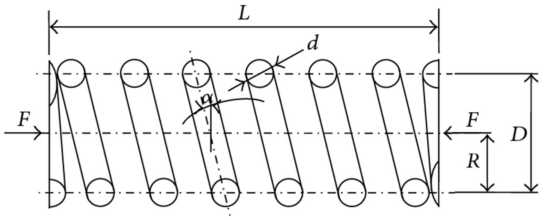

Figure 7. Spring geometrical parameters.

The shear modulus can vary consistently with temperature and phase. In Table 2, the value for NiTinol wires is reported according to [13].

Table 2. SMA properties in martensite and austenite phases.

Parameter	Value (Unit)
Austenite start temperature (A_s)	68 °C
Austenite finish temperature (A_f)	78 °C
Young's modulus, Martensite phase $(E^M{}_{SMA})$	28 GPa
Young's modulus, Austenite phase $(E^A{}_{SMA})$	75 GPa
Shear modulus, Martensite phase $(G^M{}_{SMA})$	10.56 GPa
Shear modulus, Austenite phase $(G^A{}_{SMA})$	28.20 GPa
Poisson ratio ν_{SMA}	0.33

At G(T), the shear modulus at temperature T and δ_L restricted displacement.

The shape memory alloy provided by Memory Metalle GmbH has an activation temperature of 65 °C (Alloy M, under free conditions), beyond which there is the recovery of the refined shape and, therefore, the generation of a pulling force on the sealing pin. The achievement of the target temperature for activation under operating conditions will be guaranteed by solar and/or lunar regolith radiation, which will affect the spring itself, causing a change in temperature. Note that the alloy must be chosen once the mission parameter is determined, in particular, the landing site.

The SMA spring has been manufactured following the typical procedure for the realization of SMA springs, with the aim of "memorizing" the shape that the spring will take after activation; the process is called shape-setting (Figure 8). The wire has been manually rolled up on a steel mandrel of 5 mm diameter, choosing the number of turns as needed, then the ends of the wire are locked in the final position on the rod with special grabs. The whole system is inserted into an oven at a temperature of 500 °C for 300 s; after that, the system containing the spring is quenched in cold water.

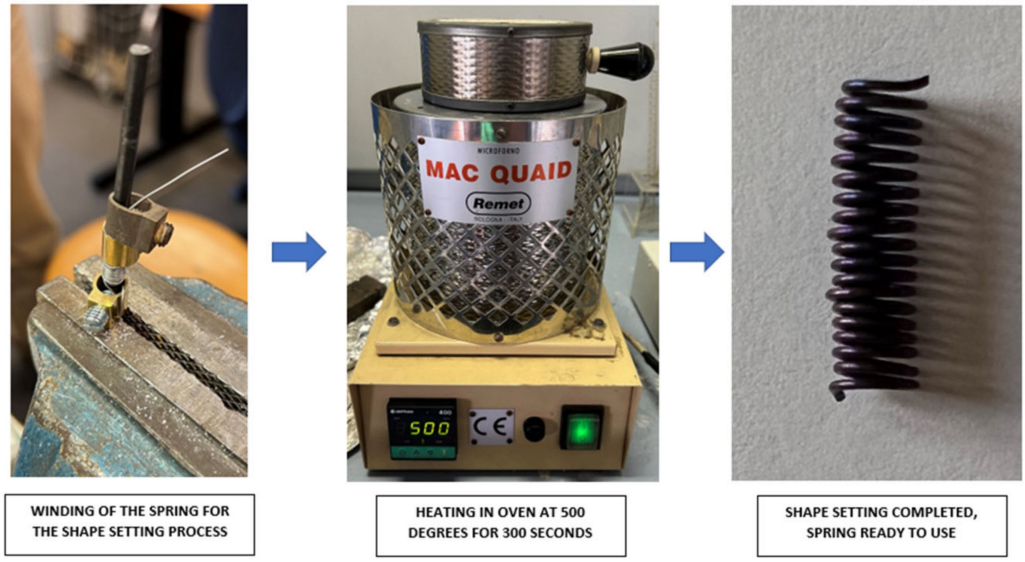

Figure 8. Shape setting process phases: wire locking on the screw, heating in the oven at 500 °C, final spring with shape memory effect after quenching in water.

2.4. SMA Spring Characterization

The manufactured SMA spring has been tested to characterize its mechanical performance with an MTS Insight® Electromechanical Testing System equipped with an environmental chamber. The system is interfaced with the TestWork application software, with test definition, execution, and report generation capabilities.

The spring was clamped in the grips of the testing system (Figure 9), and the chamber was set at T = 80 °C, a temperature higher than the whole transformation temperature. After a period of stabilization, the spring was strained with steps of 2 mm up to a maximum of 26 mm, and then back to its unstrained position in order to identify the hysteresis. Three complete loading–unloading runs were performed. Figure 10 represents the average value of the three tests. The residual displacement of the spring is close to zero after complete unloading. This phenomenon illustrates that the spring has a perfect recentering ability. The hysteresis generated by different energy dissipation in the loading and unloading phases normally does represent a challenging problem in applications where control is crucial. In application, which is the object of this paper, this is not an issue, being the operation of the device is a one-way, single-shot actuation, which ends its function after releasing the CCR package.

Figure 9. Grips system.

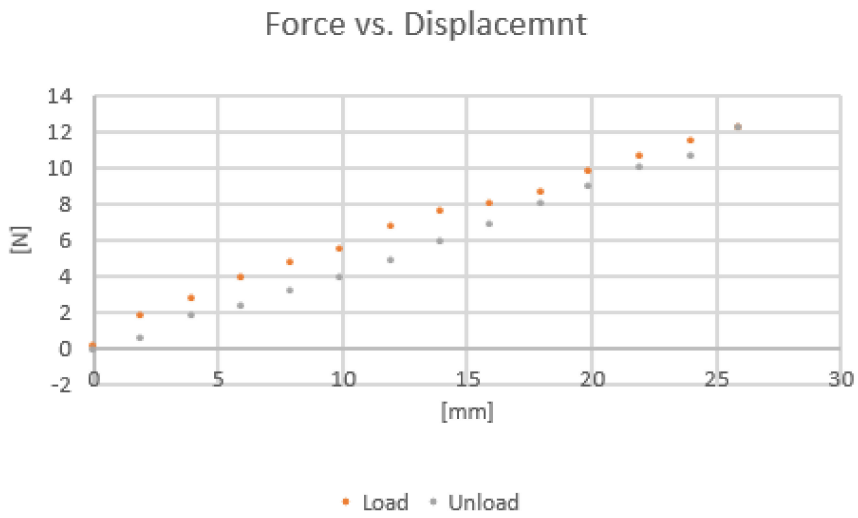

Figure 10. SMA spring force vs. displacement values.

The maximum force produced by the spring is about 13 N for a deformation of 25 mm. In order to evaluate the safety factor (SF) of the SMA spring, the force produced is considered in the position at which the sealing pin unlocked the retainer pin, which has a diameter of 5 mm. With this assumption, the force to be considered is the one for a deformation of 20 mm, which is about 10 N, resulting in an SF of 3.4.

2.5. Elegant Bread Board (EBB) Model Test

An EBB (a model defined between a bread board and an engineering model) has been built in commercial PLA with a 3D printer in order to validate the concept. For the activation of the spring, a Bosh GHG 20–63 heat gun was used with a set temperature of 100 °C, and the hot air flow was directed on the SMA spring from a distance of 300 mm. Despite careful handling needed, mainly due to the inadequate stiffness of some elements and their tendency to melt under the heat flow, the EBB demonstrated that the SMA spring was adequately designed and built and can trigger the actuator as needed (see Figure 11) by disengaging the locking pin after a contraction of 5 mm, corresponding to the diameter of the locking pin itself.

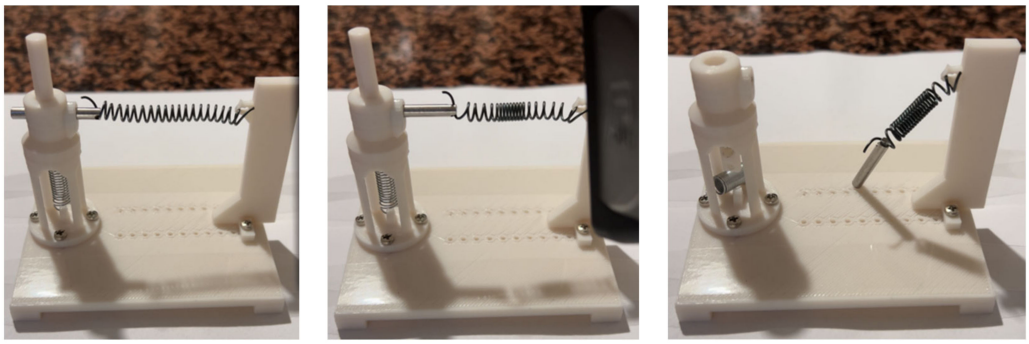

Figure 11. EBB triggering sequence.

2.6. Preliminary Emittance Measurement of the NiTinol Alloy with an IR Camera

The crucial properties of the SMA in this project are its thermo-optical properties. Emittance and solar absorptance must be well identified, and no matter what is the landing site, thermal radiation from and to the lunar regolith will be dominant in the thermal passive control mechanism, which will be responsible for the SMA spring behavior.

Some data are available in the literature on NiTinol [14,15], but during the heat treatment, the alloy further oxidizes. Some data are available in the literature on Ti oxide [16]. Although all values reported are believed to be representative of those used for thermal design, no guarantee of their validity is implied. In cases where the thermal design relies mostly on these parameters, measurements of the surface optical properties and/or a solar-thermal balance test of the thermal design must be conducted to verify the flight performance [17]. Several methods, instruments, and standards are available, and normally a dedicated specimen of the same composition and treatment status must be prepared with a suitable geometry. At this stage, a basic measurement for a preliminary evaluation of the emittance making use of a FLIR X6901sc SLS IR camera has been applied.

Knowing the temperature of the specimen (fixing all the parameters: ambient temperature, distance, relative humidity) by adjusting the input of the emittance in the instrument up to the point that the temperature of the specimen read on the IR camera coincides with the nominal temperature of SMA activation (T= 65 °C) allows defining the emittance of the specimen in the thermogram (Figure 12).

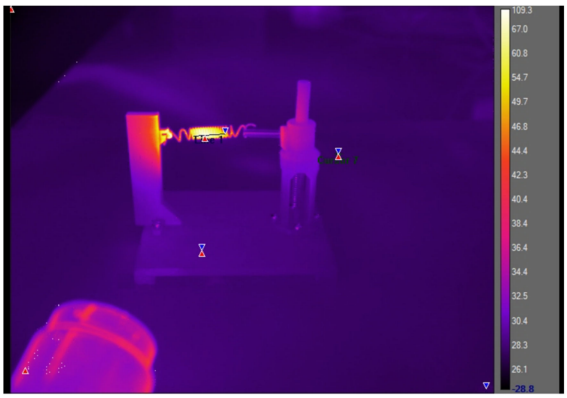

Figure 12. Thermogram of the actuator set up during the SMA spring.

With this method, a preliminary value of $\varepsilon = 0.93$ was directly measured on the SMA spring. This value represents an overestimate of a Ti oxide layer, probably due to the internal latent heat of the martensitic phase transition [18,19]. In the future, specimens with a suitable geometry must be prepared in order to measure both the emittance and solar absorptance with a dedicated instrument, such as the 410-Vis-IR Portable Emissometer & Solar Reflectometer produced by the Surface Optics Corporation (San Diego, CA, USA) and available at LNF.

The test has put evidence that in designing an engineering model, the thermal insulation of the SMA spring should be taken into account.

3. Results

In the present study, different elements of the EBB actuator for the lock and release mechanism of the NGLR experiment's CCR package were designed, built, and tested. In detail:

1. The pulling force needed to remove the sealing pin in Figure 4 was measured;
2. As a consequence, the SMA spring of the actuator was designed and built, and its characterization confirmed a pulling force of the SMA spring with an SF > 3.4;
3. The structure of the EBB of the actuator was 3D printed, and the activation of the SMA spring with a heat gun demonstrated the adequate design of the SMA spring;
4. A preliminary emittance measurement of the NiTinol alloy with an IR camera was performed, and the results are compatible with the limited literature and the geometrical and physical condition of the measured surface.

4. Discussion and Conclusions

The activation experiments performed on the prototype look promising. Its layout is simple, compact, and easily integrated into the mechanical arrangement of the whole experiment and/or the lander deck. Nonetheless, since the design foresees the activation of the SMA spring by Sun and/or Moon regolith radiation, this represents a challenge for an SMA actuator, and the thermal design of the system, the mission profile, the landing site, and the layout of the spacecraft (to be defined), will be crucial.

In addition, the setup of the actuator, in its stowage configuration, must withstand the dynamic load environment of the launch and landing phases while providing structural support to the NGLR experiment. These capabilities must be evaluated, too, once the mission profile is defined in more detail.

In the development toward a higher grade of technical maturity of the actuator, toward the design of an EM and beyond, an unavoidable consideration about how extreme the lunar environment can be against this mechanism must be evaluated [20–22], and the subsequent mitigation technologies in the design of a higher grade model must be implemented [23–25].

Author Contributions: All authors contributed equally to the different steps: conceptualization, methodology, software, formal analysis, investigation, resources, data curation, writing, review, and editing. All authors have read and agreed to the published version of the manuscript.

Funding: This research received no external funding.

Data Availability Statement: Not applicable.

Acknowledgments: Not applicable.

Conflicts of Interest: The authors declare no conflict of interest.

References

1. Turyshev, S.G.; Williams, J.G.; Folkner, W.M.; Gutt, G.M.; Baran, R.T.; Hein, R.C.; Somawardhana, R.P.; Lipa, J.A.; Wang, S. Corner-cube retro-reflector instrument for advanced lunar laser ranging. *Exp. Astron.* **2012**, *36*, 1052013–1052135. [CrossRef]
2. Delle Monache, G.O.; Tata, M.E. Development of a magnetic cardan suspension coupled with a single actuated axis for gravity-assisted pointing of directional devices: A case study of Moon to Earth alignment for a laser ranging retroreflector. *Adv. Space Res.* 2022, in press. [CrossRef]
3. Dietz, R.H.; Rhoades, D.E.; Davidson, L.J. *Apollo Experience Report—Lunar Module Communication System*; NASA TN D-6974; NASA Manned Spacecraft Center: Houston, TX, USA, 1972.
4. Costanza, G.; Tata, M.E.; Libertini, R. Effect of temperature on the mechanical behaviour of Ni-Ti shape memory sheets. In Proceedings of the 145th Annual Meeting and Exhibition, TMS, Nashville, TN, USA, 14–18 February 2016; pp. 433–439.
5. Costanza, G.; Tata, M.E.; Calisti, C. Nitinol one-way shape memory springs: Thermomechanical characterization and actuator design. *Sens. Act. A* **2010**, *157*, 113–117. [CrossRef]

6. Costanza, G.; Tata, M.E. Shape Memory Alloys for Aerospace, Recent Developments, and New Applications: A Short Review. *Materials* **2020**, *13*, 1856. [CrossRef] [PubMed]
7. Razov, A.; Cherniavsky, A. Applications of shape memory alloys in space engineering: Paste and future. In Proceedings of the 8th European Space Mechanisms and Tribology Symposium, European Space Agency ESA-SP, Toulouse, France, 29 September–1 October 1999; Volume 438, p. 141.
8. Tsushiya, K.; Koyano, T.; Todaka, Y.; Umemoto, M. Development of shape memory actuator for cryogenic application. In *Next-Generation Actuators Leading Breakthroughs*; Springer: London, UK, 2009.
9. Badescu, M.; Bao, X.; Bar-Cohen, Y. Shape memory alloy (SMA)-based launch lock. In Proceedings of the Proceedings Volume 9061, Sensors and Smart Structure Technologies for Civil, Mechanical and Aerospace Systems, San Diego, CA, USA, 10–13 March 2014; Volume 961.
10. Hanon, M.M.; Zsidai, L. Comprehending the role of process parameters and filament color on the structure and tribological performance of 3D printed PLA. *J. Mater. Res. Technol.* **2021**, *15*, 647–660. [CrossRef]
11. Savi, M.A.; Pacheco, P.; Garcia, M.S.; Aguiar, R.A.A.; de Souza, L.F.G.; da Hora, R.B. Nonlinear geometric influence on the mechanical behavior of shape memory alloy helical springs. *Smart Mater. Struct.* **2015**, *24*, 035012. [CrossRef]
12. Ma, J.; Huang, H.; Huang, J. Characteristics Analysis and Testing of SMA Spring Actuator. *Adv. Mater. Sci. Eng.* **2013**, *2013*, 823594. [CrossRef]
13. Rodrigue, H.; Wei, W.; Bhandari, B.; Ahn, S.-H. Fabrication of wrist-like SMA-based actuator by double smart soft composite casting. *Smart Mater. Struct.* **2015**, *24*, 125003. [CrossRef]
14. Da Silva, T.C.; Costa Sá, M.V.; Da Silva, E.P.; Da Silva, F.C. Emissivity Measurements on Shape Memory Alloys. In Proceedings of the Quantitative InfraRed Thermography Conference, Quebeck, QC, Canada, 4–8 July 2016. [CrossRef]
15. Costanza, G.; Paoloni, S.; Tata, M.E. IR thermography and resistivity investigations on Ni-Ti shape memory alloy. *Key Eng. Mater.* **2014**, *605*, 23–26. [CrossRef]
16. Kauder, L. *Spacecraft Thermal Control Coatings NASA/TP–2005–212792*; Technical Publication NASA/Goddard Space Flight Center: Greenbelt, MD, USA, 2005.
17. Gilmore, D.G. *Spacecraft Thermal Control Handbook*, 2nd ed.; Volume 1: Fundamental Technologies; The Aerospace Press: El Segundo, CA, USA, 2002; ISBN 1-884989-11-X.
18. Kato, H. Latent heat storage capacity of NiTi shape memory alloy. *J. Mater. Sci.* **2021**, *56*, 8243–8250. [CrossRef]
19. Armattoe, K.; Bouby, C.; Haboussi, M.; Ben Zineb, T. Modeling of latent heat effects on phase transformation in shape memory alloy thin structures. *Int. J. Solids Struct.* **2016**, *88-89*, 283–295. [CrossRef]
20. Gaier, J.R. *The Effects of Lunar Dust on EVA Systems During the Apollo Missions, NASA/TM—2005-213610*; Technical Memorandum NASA/Glenn Research Center: Cleveland, OH, USA, 2005.
21. Stubbs, T.J.; Vondrak, R.R.; Farrell, W.M. Impact of dust on lunar exploration. In *Dust in Planetary Systems, ESA SP-643*; NASA Astrophysics Data System: Kauai, HI, USA, 2007.
22. Heiken, G.H.; Vaniman, D.T.; French, B.M. *Lunar Sourcebook, 3.4. Dust*; Cambridge University Press: Cambridge, UK, 1991; ISBN 0-521334446.
23. Budzyń, D.; Tuohy, E.; Garrivier, N.; Schild, T.; Cowley, A.; Cruise, R.; Cammarano, A. Lunar dust: Its impact on hardware and mitigation technologies. In Proceedings of the 46th Aerospace Mechanisms Symposium, Virtual, 11–13 May 2022.
24. Chakrabarti, A. *Engineering Design Synthesis: Understanding, Approaches and Tools*; Springer: London, UK, 2002; ISBN 978-1852334925.
25. Cannon, K.M.; Dreyer, C.B.; Sowers, G.F.; Schmit, J.; Nguyen, T.; Sanny, K.; Schertz, J. Working with lunar surface materials: Review and analysis of dust mitigation and regolith conveyance technologies. *Acta Astron.* **2022**, *196*, 259–274. [CrossRef]